JAAS

Accepted Manuscript

This is an *Accepted Manuscript*, which has been through the Royal Society of Chemistry peer review process and has been accepted for publication.

Accepted Manuscripts are published online shortly after acceptance, before technical editing, formatting and proof reading. Using this free service, authors can make their results available to the community, in citable form, before we publish the edited article. We will replace this *Accepted Manuscript* with the edited and formatted *Advance Article* as soon as it is available.

You can find more information about *Accepted Manuscripts* in the Information for Authors.

Please note that technical editing may introduce minor changes to the text and/or graphics, which may alter content. The journal's standard Terms & Conditions and the Ethical guidelines still apply. In no event shall the Royal Society of Chemistry be held responsible for any errors or omissions in this *Accepted Manuscript* or any consequences arising from the use of any information it contains.

ROYAL SOCIETY OF CHEMISTRY

www.rsc.org/jaas

Precise Analysis of Calcium Stable Isotope Variations in Biological Apatites using Laser Ablation MC-ICPMS

Théo Tacail[1]*, Philippe Télouk[1], Vincent Balter[1]

[1] Laboratoire de Géologie de Lyon: Terre, Planète, Environnement, UMR CNRS 5276 (CNRS, ENSL, Université Lyon 1), Ecole Normale Supérieure de Lyon, 69364 Lyon cedex 07, France

* Corresponding author email: theo.tacail@ens-lyon.fr

Keywords: laser ablation; calcium stable isotopes; bioapatite; fluorapatite; enamel

Laser ablation (LA) is potentially an interesting technique to measure calcium isotopes natural variations ($\delta^{44/42}$Ca) in calcium-rich minerals because it allows spatial resolution and avoids micro-sampling and consecutive wet chemistry. We developed a matrix-match sample/standard normalization method and used an Excite 193 nm Photon Machines LA system coupled to a Neptune *plus* MC-ICPMS to measure $\delta^{44/42}$Ca variations in enamel apatite. First, high precision $\delta^{44/42}$Ca solution mode (SOL) analyses were performed on a series of 5 crystalline igneous apatite and 6 modern tooth enamel samples, which were micro-sampled using a MicroMill device. The $\delta^{44/42}$Ca isotopic values ranged evenly between - 0.60 and + 0.60 ‰ (per amu). Second, we sintered by means of spark plasma sintering technique the bone ash SRM1400 standard and two synthetic apatites (doped or not with Sr). The Ca isotope compositions using LA were measured in the samples in the raster mode along 600x85 µm profiles and bracketed with the SRM1400 standard. We obtained a very good agreement between SOL and LA measurements, i.e. $\delta^{44/42}Ca_{LA}$ vs $\delta^{44/42}Ca_{SOL}$ slope of 0.960 ± 0.091 (2SE, R^2 = 0.971) and null offset at origin (0.012 ± 0.084, 2SE). For all samples, residual values to the 1:1 slope were ≤ 0.1 ‰ (per amu). However, an unexplained and constant 0.13 ‰ offset occurred when considering the $^{43/42}$Ca ratio, suggesting an uncorrected isobaric interference on ^{43}Ca in the LA mode. We also noticed that the doubly charged strontium (Sr) interference correction is of crucial importance for accurate matching between LA and SOL measurements. In the SOL mode, Sr is discarded by ion chromatography leading to typical $^{87}Sr^{2+}/^{44}Ca^{+}$ ratios of 10^{-5} to 10^{-6}. In the LA mode, this ratio can exceed 10^{-3}. We show that the value set for the ^{87}Sr/^{86}Sr ratio is of importance to correct the Sr interference, and that optimized residuals to the 1:1 slope are obtained using a Sr correction that takes into account a mass fractionation factor for doubly charged Sr distinct from that of Ca. We found that deciduous teeth enamel is depleted in Ca heavy

isotopes by about 0.35-0.40 ‰ (per amu) compared to wisdom teeth enamel, a shift compatible with a transition from a milk based diet to a plant and meat based diet.

1. Introduction

The Ca stable isotope compositions of biological hydroxylapatites (bioapatite) and especially of fossil teeth enamel constitute a promising tool for paleodietary studies, because a stepwise trophic level effect has been described in marine, and to a lesser extent, in continental environments.[1-7] In addition, the Ca isotope composition of milk is one of the most ^{44}Ca-depleted materials reported so far.[5,8] Although not demonstrated yet, physiological stresses or early-life dietary transitions can influence the body Ca isotope burden, the resulting variations of which being potentially recorded spatially in enamel. This suggests that the weaning period could be defined by a shift towards heavier Ca isotopic values along enamel growth prisms. These applications would notably benefit from the development of a quasi non-destructive *in situ* method, adapted to the analysis of precious fossils, whilst allowing an increased spatial resolution and no compromising analytical precision.

In situ measurements of stable isotope ratios by laser ablation multi-collector inductively-coupled plasma mass spectrometry (LA-MC-ICPMS) is restricted to a few elements so far, mainly iron[9-18], magnesium[15,18-20], silicon[20,21], copper,[9,22] sulphur[23] and boron[24], and is mainly applied to characterization of silicate glasses and minerals, oxides, metals, allies and sulphides. Laser ablation (LA) technique faces a series of technical hindrances to accurate and precise stable isotope ratios measurements, among which LA induced fractionation, unresolved isobaric interferences and a serious lack of solid matrix-matched homogeneous standards certified for isotopic compositions. The multiple elemental and isotopic fractionation effects associated to LA technique take place during vaporization and condensation at the ablation site, during transport of resulting heterogeneously sized particles

and in the plasma during incomplete atomization and ionization of particles.[11,12,14,22] These effects strongly depend on the nature of the ablated material and thus require matching of matrices between standards and samples in terms of chemical composition and mineralogy, especially when considering nanoseconds LA systems.[9,13,20,24,25]

We present here the first method described for Ca isotope determination by LA-MC-ICPMS on enamel bioapatite that solves these problems and fulfils mass-dependent fractionation, accuracy and precision requirements. We developed a strategy based on a matrix-matched standard-bracketing normalization and an extensive doubly charged Sr interferences correction. This strategy is applied to a series of macrocrystalline igneous fluorapatites (FAP) as well as synthetic and biogenic microcrystalline hydroxylapatites (HAP), previously measured for their Ca isotope composition using classical wet chemistry (hereafter noted solution or SOL mode).

2. Material

We selected various natural geologic and biological apatites, with various crystallite sizes and isotopic compositions, as described in Table 1A. Standards for LA measurements were prepared in order to achieve matching of matrices between standards and samples in terms of mineralogy and Sr contents.

2.1. Samples

A series of five igneous centimetre long monocrystalline FAP from various locations (Burma, Brazil, Mexico, Madagascar and Morocco, Table 1A) were selected. These igneous materials are expected to have quite high $\delta^{44/42}$Ca values[1,4] and to be isotopically homogeneous at the crystal scale. Igneous apatites were cut in thin slices and small chips of approximately 1 mg were sampled for analysis in the SOL mode. Remaining FAP crystals

were included in araldite and resulting mounts were cleaned using wet fine-grained sandpapers.

Sample abbreviation	Description
A - Samples	
BRM	Natural igneous monocristalline FAP, Burma
BRZa	Natural igneous monocristalline FAP, Brazil
DUR	Natural igneous monocristalline FAP Durango, Mexico
MD1	Natural igneous monocristalline FAP, Madagascar
MRCa	Natural igneous monocristalline FAP, Morocco
BMM3	Female wisdom 3^{d} molar tooth enamel ***
HPME	Female wisdom 3^{d} molar tooth enamel
BME1	Female deciduous canine tooth enamel
BMC	Female deciduous canine tooth enamel ***
PBC	Male deciduous canine tooth enamel ***
VBI	Male deciduous incisor tooth enamel ***
B - SOL mode standards	
ICP Ca Lyon **	ICP Alfa Aesar 10'000 µg L^{-1} Ca Solution[1]
SRM915b	Clinical Grade Carbonate NIST Standard Reference Material
SRM1486	Bone Meal NIST Standard Reference Material
Seawater	Seawater sample from Belize near shore
CBE	Cave Bear Enamel powder in-house standard[1]
C - LA mode standards	
SRM1400	Bone Ash Hydroxyapatite NIST SRM powder
SRM1400-SPS *	Bone Ash Hydroxyapatite NIST SRM sintered using SPS technique
SRM1400-gold	Bone Ash Hydroxyapatite NIST SRM belt sintered using belt technique[2]
HAPp1-SPS	SPS sintered powder synthetic Hydroxyapatite
HAPp2-SPS	SPS sintered powder synthetic Hydroxyapatite doped with Sr

Table 1: Samples (A.) and Standards for both Solution (B.) and Laser Ablation (C.) MC-ICPMS modes analyses [1] Described in Tacail *et al.*[34], [2] Described in Balter and Reynard[32], Balter *et al.*[31] and Balter *et al.*[33], * used as LA mode bracketing standard, ** used as SOL mode bracketing standard, *** sample obtained using MicroMill

Two wisdom and four deciduous human teeth from four different living individuals (Table 1A) were also selected. Tooth enamel samples are expected to have quite low $\delta^{44/42}$Ca values[*e.g.* 2,3,5,7] together with possible individual or tooth type specificities. Once included in araldite, resulting mounts were cut and polished across the tooth vertical bucco-lingual plane

for LA mode analyses. Chips of HPME and BMM3 enamel were sampled for analysis in the SOL mode on the other halves of teeth. For the 4 other teeth, a MicroMill device was used for precise position drilling with a 400 µm diameter tungsten carbide drill. Drill holes were approximately 400 µm in diameter and 300 µm in depth. Small powder heaps were collected using two clean razorblades and introduced into 7 mL Teflon beakers. Enamel surface, drill bit and razorblades were washed with 99 % pure ethanol and blown off using compressed air duster between each drilling. A single drilling allowed recovering of approximately 80 µg HAP corresponding to about 30 µg Ca.

2.2. SOL mode standards

Precision and accuracy of solution mode measurements were estimated by measuring isotopic compositions of several international and in-house Ca isotope standards listed in Table 1B.

2.3. LA mode standards

The standards used in the LA mode are listed and described in Table 1C. The SRM1400 standard was used as the main reference standard for the LA mode. It is a cattle bone ash NIST Standard Reference Material powder certified or well described for major and trace elements concentrations and for Pb and Sr radiogenic ratios[26-28] but for which no Ca isotopic composition has been proposed yet. This standard, which contains no or very little organic matter, consists in nano- to microcrystalline HAP that resembles enamel crystallites.

In order to better control the Sr doubly charge effects on the Ca isotope composition, we carried out two experiments of apatite precipitation following the procedure described in Balter & Lécuyer [29]. Briefly, HAPp1 was synthetized by mixing 1 L of $CaCl_2 \cdot 4H_2O$ at 2.6×10^{-2} mol.L^{-1} and 1 L of $Na_2HPO_4 \cdot 2H_2O$ at 2.5×10^{-2} mol.L^{-1}. For both initial solutions, pH was set at 10.8 by adding 1 M NaOH. For the second precipitation experiment (HAPp2), 4 mg Sr from Alfa Aesar ICP 10'000 ppm solution were added to the $CaCl_2 \cdot 4H_2O$ prior to

pH adjustment. Resulting precipitates were constantly agitated in reaction vessels and kept at 25 °C during 96 h for crystals maturation. At the end of the experiments the supernatant was discarded after centrifugation in 500 mL centrifugation vials. Precipitates were freeze-dried to avoid subsequent modification of crystallites and finally homogenized in an agate mortar.

Powders of SRM1400, HAPp1 and HAPp2 were sintered using Spark Plasma Sintering technique (SPS), which consists in applying a pulsed electric current simultaneously with compressive stress to a die containing initial powder sample.[30] The rapid and efficient heating enabled by the current applied to the powder allows coalescence of grains without major phase changes at temperatures up to 1200 °C and pressure less than 100 MPa.[30] The SPS technique allows drastic reduction of porosity and thus leads to sintered materials yielding more than 98 % of theoretical maximal density. The sintering of SRM1400, HAPp1 and HAPp2 powders was carried out at the INSA Lyon MATEIS Laboratory using a FCT system HP D 25 SPS apparatus (Germany). The SPS runs were carried out in vacuum sintering atmosphere (3 x 10^{-1} mbar) at the following operating conditions:[30] compressive stress was set at 75 MPa, temperature increased at a rate of 100 °C.min^{-1} and plateaued at 900 °C during 3 to 4 min until shrinkage rate was null. The SRM1400 standard used in previous studies by Balter[31-33] was also analysed in the LA mode to test for possible effect of the sintering technique. This standard, here labelled "SRM1400-gold", was sintered at 2 GPa and 700 °C in a belt apparatus at the Centre des Hautes Pressions of the Claude Bernard Lyon1 University. Prior to LA analysis, all sintered standards were included in araldite resin and polished to obtain flat surfaces and remove superficial impurities such as graphite from SPS dies.

In parallel with the preparation of the SPS standards (written with “-SPS” suffix hereafter), SRM1400, HAPp1 and HAPp2 powders were sampled for precise analysis in the SOL mode. The SRM1400-SPS sintered standard was also micro-sampled for precise SOL

mode analysis using MicroMill in order to check for any influence of the sintering process on the Ca isotope composition.

Settings	A. SOL mode	B. LA mode
Aridus II		
Sweep Gas Flow (Ar) [L min-1]	7-9	7-8
Nitrogen Gas Flow [mL min-1]	5-8	4-6
Spray Chamber Temp. [°C]	110	
Desolvator Temp. [°C]	160	
Aspiration type	free	
Uptake rate [µL min-1]	120	
Ca concentration [mg L-1]	1.5 - 3.0	-
Thermo Neptune *plus*		
RF power [W]	1200	
Cool gas [L min-1]	15	
Aux Gas [L min-1]	0.7	
Sample Gas [L min-1]	0.95 - 1.20	
Extraction [V]	-2000	
Acceleration potential [V]	-10000	
Sampler Cone	Jet	Standard
Skimmer Cone	X	H
Resolution slit	MR	HR
Faraday Cups Configuration And Resitances [Ω]	L4 - $^{42}Ca^{+}$ - 10^{11} Ω L2 - $^{43}Ca^{+}$ - 10^{12} Ω L1 - $^{87}Sr^{2+}$ - 10^{11} Ω C - $^{44}Ca^{+}$ - 10^{11} Ω	
Excite 193nm LA system		
Cell type	-	Helex Chamber
LA pulse width	-	< 4 ns
He carrier MFC1 Flow [L min-1]	-	0.900
He carrier MFC2 Flow [L min-1]	-	0.400
Maximal Fluence [J cm-1]	-	15.2
Delivered Fl. [% of max. Fl.]	-	70 - 100
Raster Scan lengths [µm]	-	500 - 600
Scan speed [µm s-1]	-	10
Spot size (diameter) [µm]	-	85
Repetition rate [Hz]	-	15
Washout time [s]	-	30

Table 2: Optimized settings of MC-ICPMS Thermo Neptune *plus* and LA Excite system for both SOL (A.) and LA (B.) modes

3. Analytical Methods

3.1. SOL mode analysis

A two-step chemical purification of samples was performed following the method described in Tacail *et al.*[34] Briefly, once digested, samples were processed through AG50W-X12 cationic resins in 1 N HCl medium for matrix discard. Calcium was recovered together

with Sr in 6 N HCl and processed through Sr specific resins (Sr Spec) in 2 N HNO_3 medium for Sr elimination. The measurements of Ca isotope ratios in the SOL mode were carried out at the ENS-Lyon using a Neptune *plus* MC-ICPMS (Thermo Scientific, Bremen, Germany) following method described in Tacail *et al.*[34] Optimized operating parameters for SOL mode analyses are summarized in Table 2A. Each analysis was preceded by a washout pumping in 0.5 N HNO_3 using the Aridus quickwash module. A second washout pumping was carried out in 0.05 N HNO_3 and measured as blank, this background being subtracted online before calculation of isotope ratios. The ICP Ca Lyon standard[34] was used as SOL mode bracketing standard. All Ca isotopes compositions are expressed using the delta notation defined as follows for $\delta^{44/42}$Ca:

$$\delta^{44/42}Ca = \left(\frac{R_{sple}^{44/42}}{R_{std}^{44/42}} - 1\right) \times 1000 \qquad \text{[Eq. 1]}$$

where $R^{44/42}$ stands for measured $^{44}Ca/^{42}Ca$ ratios and *sple* and *std* subscripts refer to sample and standard respectively. Either ICP Ca Lyon or SRM1400 are used as reference standard for delta notation and are specified with subscripts *ICP* or *SRM* thereafter.

3.2. LA mode analysis

Analyses in the LA mode were carried out using an Excite 193 nm ArF Excimer laser system (Photon Machines, MT, USA) delivering 4 ns pulses at a maximal fluence of 15.2 $J.cm^{-1}$. The mounted HeLex cell allowed ablation of samples in ultra-pure He atmosphere with efficient recovering of ablated material. The LA system was connected to the plasma torch *via* Teflon tubing in series with a "squid" signal-smoothing device. A T-piece adapter allowed mixing of He carrier gas with an Ar makeup gas flow from Aridus II in order to ensure plasma ignition and stability. Although this desolvating system drastically reduces the amount of transmitted water, it allowed either moderate addition of moist from freely

aspirated and nebulized distilled 0.05 N HNO_3 during LA mode analyses, or introduction of Ca from ICP Ca Lyon solution for daily pre-tuning of MC-ICPMS.

The optimized LA mode operating parameters of MC-ICPMS and LA system are summarized in Table 2B. Faraday cups configurations were identical to SOL mode. As doubly charged Sr isotopes constitute unresolvable interfering species on all three measured Ca isotopes beams,[34] L1 faraday cup was also set for collection of m/z = 43.5 beams, corresponding to measurement of $^{87}Sr^{2+}$ signal. Contrarily to SOL mode, where nickel Jet-X sampler and skimmer cones were used,[34,35] LA mode analyses were performed with a Standard-H pair, although Jet interface allows an average 5-fold transmission increase. This combination permitted reduction of polyatomic species formation at the cone interface, such as molecular oxides, hence reducing potential isobaric interferences or instabilities.[*e.g.* 36]

As described elsewhere,[34,37] measurements of $^{42}Ca^+$, $^{43}Ca^+$ and $^{44}Ca^+$ signals are hindered by numerous polyatomic isobaric interferences, largely caused by Ar from introduction gas, O_2 and N_2 from air and H_2O from dilute acids. These interferences constrain the measurement of Ca isotopic ratios to the left shoulder of the Ca peak, especially because of the interference of $^{40}Ar^1H_2^+$ with $^{42}Ca^+$. Calcium isotopes measurement by MC-ICPMS requires a minimal resolving power of 2 200 in order to perform measurement in a 10^{-2} amu wide window,[37] which is achieved by the use of the Medium Resolution mode of (MR mode). Concerning analyses in the LA mode, polyatomic interferences induced by introduction gases and water are apparently unchanged despite addition of He flow. Mass scan of blanks in the LA mode, *i.e.* with gas only and unfocused firing laser, were similar to those performed in the SOL mode using 0.05 N HNO_3 (Fig. S1). Analyses in the LA mode were performed using the High Resolution slit (HR mode) to ensure maximal resolution and stability of central mass position.

Daily tuning of MC-ICPMS consisted in a primary gross tuning of transmission, peak shape and peak centering using ICP Ca Lyon introduced *via* Aridus II and in a second refined

tuning performed by ablating SRM1400-SPS along a continuous raster. This allowed optimization of Aridus II and He gas flows, torch position, source lenses and zoom optics.

Laser ablation scan speed, repetition rate and effective fluence were optimized for Ca transmission and signal stability, but were not found to have specific impact on the measured Ca isotopes ratios. Spot diameter was set at 85 µm in order to ensure sufficient Ca transmission, notably in order to overcome influence of potentially unresolved constant polyatomic isobaric interferences induced by introduction gases.

In this study, scan line ablations were preferred to spot ablation because of strong transient laser induced fractionation described for spot ablation on several isotopic systems, especially regarding nanosecond UV LA when compared to femtosecond UV LA.[11,22-25] Although it is not sure whether these transient isotopic effects are linked to heterogeneous particle sizes or to fractionation effects occurring at the ablation site and/or in the plasma, scan lines allow reaching steady state in both transport of different particle types and fractionation effects. Ablation lines of about 500 to 600 µm were thus performed in order to quickly obtain intensities and measured ratios as steady as possible.

The ablation and acquisition procedure was performed as follows. Ablation sequence was prepared using the LA system software (*Chromium 2*) and consisted in a fine optical focus on sample surface together with a precise positioning of scan lines. Acquisition method was set to acquire an infinite number of 1.049 s lasting integration cycles. Sample ablations were preceded by blank acquisition, implying unchanged Ar and He gas flows combined with unfocused laser firing on a sample-free zone. Sequences consisted in series of 15 to 25 ablation scans in which ablations of samples were bracketed by analyses of the SRM1400-SPS standard. Each ablation was followed by 30 s of washout, necessary to reach average blank levels. The HAPp2-SPS standard was regularly analysed as a sample in order to check

for the influence of the doubly charged Sr interference on the accuracy of the measurements on a Ca-fractionated and Sr-doped material.

All ablated materials displayed intensities within 10 % of the SRM1400-SPS typical signal, even when considering macro- *vs.* microcrystalline apatites (*i.e.* igneous FAP *vs* synthetic or biologic HAP). Typical signal intensities in these conditions are about 1.2 V, 0.3 V and 4.2 V for the $^{42}Ca^{+}$, $^{43}Ca^{+}$ and $^{44}Ca^{+}$ signals respectively, while blanks were yielding average values of 1 x 10^{-3} V, 2 x 10^{-4} V and 3 x 10^{-3} V for 42, 43 and 44 m/*z* ratios signals respectively.

Data were processed offline using an in-house python code. This program allowed isolating initial blank sections and cutting sample ablation plateaus with systematic rejection of instabilities at the signal onset. After blank subtraction, Ca isotope signals were corrected for doubly charged Sr interferences, *i.e.* $^{84}Sr^{2+}$, $^{86}Sr^{2+}$ and $^{88}Sr^{2+}$ on $^{42}Ca^{+}$, $^{43}Ca^{+}$ and $^{44}Ca^{+}$ respectively. As described in Tacail *et al.*[34], the correction consisted in subtracting inferred doubly charged $^{2x}Sr^{2+}$ contribution on $^{x}Ca^{+}$ signals. This contribution was calculated by considering that Sr isotopes are fractionated in the instrument following a mass-dependent exponential fractionation law.[38,39] Equation for correction of a given $^{x}Ca^{+}$ signal gives:

$$^{x}Ca^{+} = V_x - V_{43.5} \times \frac{^{2x}Sr}{^{87}Sr} \times \left(\frac{M_{^{2x}Sr}}{M_{^{87}Sr}}\right)^{f_{Sr^{2+}}} \quad \text{Eq. [2]}$$

where *x* equals 42, 43 or 44, V_x is the signal of m/*z* = *x* beam, $V_{43.5}$ the signal of m/*z* = 43.5 beam, $^{2x}Sr/^{87}Sr$ the natural abundances ratio of ^{2x}Sr and ^{87}Sr isotopes, $M_{^{2x}Sr}$ and $M_{^{87}Sr}$ the atomic masses of ^{2x}Sr and ^{87}Sr isotopes in atomic mass units (amu) and $f_{Sr^{2+}}$ the doubly charged Sr exponential-law mass fractionation coefficient (see section 5.2). This correction relies on two main parameters, namely the true Sr isotopic ratio and the mass-fractionation

coefficient. True $^{2x}Sr/^{87}Sr$ isotopic ratios were calculated on the basis of a radiogenic $^{87}Sr/^{86}Sr$ ratio of 0.7103, corresponding to rounded $^{87}Sr/^{86}Sr$ ratio in NBS987.[40,41,42,43,44] This ratio allows calculation of true ratios of 0.0796, 1.4079 and 11.7959 for $^{84}Sr/^{87}Sr$, $^{86}Sr/^{87}Sr$ and $^{88}Sr/^{87}Sr$ considering average natural abundances of Sr stable isotopes. Doubly charged Sr mass fractionation coefficient, $f_{Sr^{2+}}$, was estimated on the basis of accuracy optimization on the $^{44}Ca/^{42}Ca$ ratio of repeated analyses of HAPp2-SPS standard measured as sample. This sample was chosen because it has the highest Sr content of all samples and standards. Both of these parameters were used to correct for doubly charged interferences of all measured samples and standards. All $^{44}Ca/^{42}Ca$ and $^{43}Ca/^{42}Ca$ corrected ratios were then calculated for each cycle of each scan, and values deviating by more than 1SD from the mean were discarded. Average ratios of each ablation scan were then used for calculation of $\delta^{44/42}Ca_{SRM}$ and $\delta^{43/42}Ca_{SRM}$ of sample or standard.

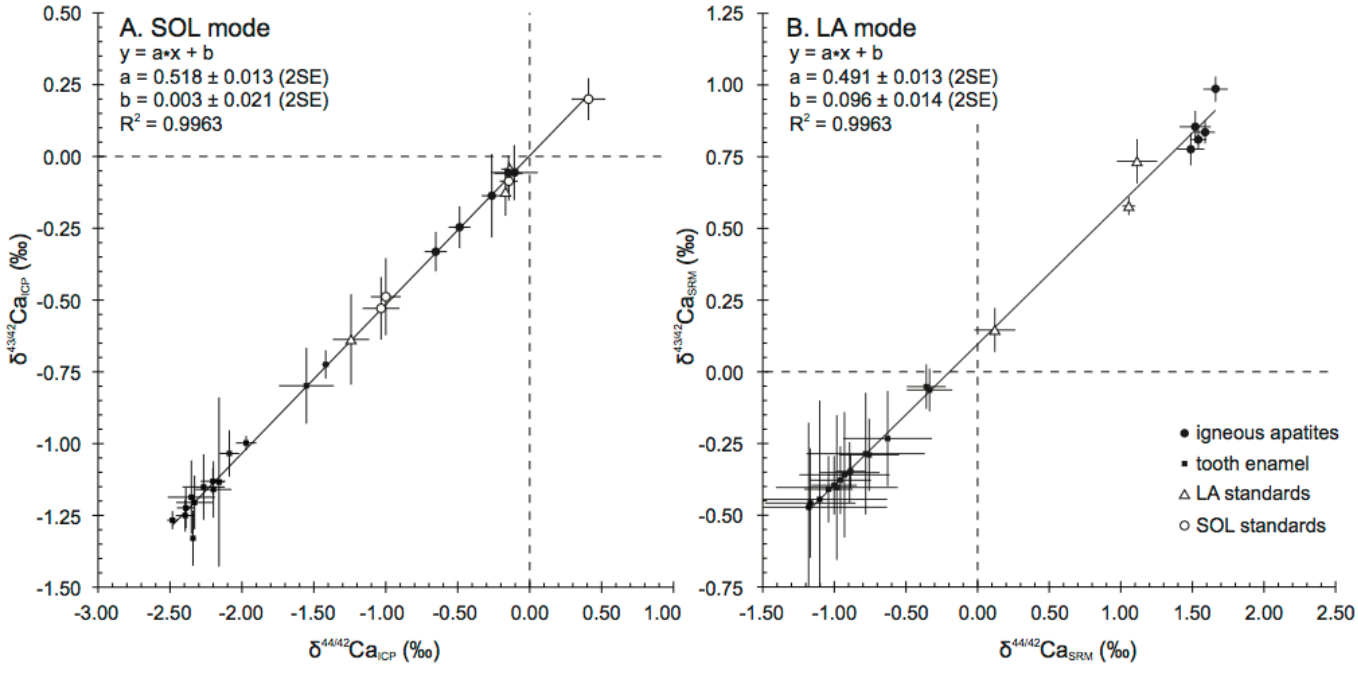

Figure 1: $\delta^{44/42}Ca$ (‰) *vs* $\delta^{43/42}Ca$ (‰) for (A) SOL mode relatively to ICP Ca Lyon Standard and (B) LA mode relatively to SRM1400. Both SOL and LA mode display strongly correlated mass fractionation lines with slopes in good agreement with predicted mass dependent fractionation (*i.e.* 0.507 according to exponential law). LA mode exhibits a constant offset at origin of 0.096 ± 0.014 ‰ likely linked to an uncorrected interference on

^{43}Ca signal. Black lines are regression lines and error bars are 2SD in SOL mode and 2SE in LA mode.

4. Results

4.1. SOL mode results

When plotted in a $\delta^{43/42}Ca_{ICP}$ *vs* $\delta^{44/42}Ca_{ICP}$ diagram (Fig. 1A), all samples and standards measured in the SOL mode fall on a line displaying a strong correlation ($R^2 = 0.9963$), a null offset at origin (0.003 ± 0.021, 2SE) and a slope of 0.518 ± 0.013 (2SE), which is in general agreement with the 0.507 value predicted by the linear approximation of exponential mass-dependent fractionation law.

The $\delta^{44/42}Ca_{ICP}$ values of the standards are given in Table 3 together with converted literature values. All measured standards – namely SRM915b, Seawater, SRM1486 and CBE – display values in good agreement with literature data and with previously published values. Long-term external reproducibility (2SD), estimated using SRM1486, yields 0.13 ‰ for $\delta^{44/42}Ca$ (n = 120). The SRM1400 standard displays a $\delta^{44/42}Ca_{ICP}$ value of - 1.24 ± 0.13 ‰ (2SD, n = 26). This first published SRM1400 Ca isotope composition falls within the domain of previously described isotopic compositions of cattle bones,[5] which yield an average $\delta^{44/42}Ca_{ICP}$ value of - 1.00 ± 0.34 ‰ (2SD, n = 25). When expressed relatively to SRM915b, the $\delta^{44/42}Ca_{915b}$ value of SRM1400 is - 1.10 ± 0.14 ‰ (2SD, n = 26). The $\delta^{44/42}Ca_{ICP}$ value remains unchanged after sintering and micro-sampling of SRM1400-SPS (- 1.18 ± 0.16 ‰, 2SD, n = 11) showing that these treatments have no effect on the Ca isotope compositions.

Results obtained in the SOL mode for samples and standards are given in Table 4 relatively to ICP and to SRM1400 for convenient comparisons with results obtained in the LA mode. The $\delta^{44/42}Ca$ dataset displays values spanning a range of 2.50 ‰, which is almost the entire natural variability described so far. The four deciduous teeth exhibit the most ^{44}Ca-depleted compositions of the dataset, with an average $\delta^{44/42}Ca_{ICP}$ of - 2.22 ± 0.21 ‰ (2SD,

n = 4) while the two wisdom teeth have less ^{44}Ca-depleted values (- 1.48 ± 0.19 ‰, 2SD). Igneous FAP represent the most ^{44}Ca-enriched apatites, with notably MD1 yielding a value of - 0.11 ± 0.16 ‰ (2SD, n = 6). Synthetic apatites HAPp1 and HAPp2 display quite ^{44}Ca-enriched compositions as well, with $\delta^{44/42}Ca_{ICP}$ values of - 0.14 ± 0.06 ‰ (n = 2) and - 0.17 ± 0.01 ‰ (n = 2) respectively, corresponding to - 1.10 ± 0.06 ‰ (n = 2) and - 1.07 ± 0.01 ‰ (n = 2) when expressed relatively to SRM1400.

Study	Instrument	SRM915a	SRM915b	Seawater	SRM1486	CBE	SRM1400
This study	**MCICPMS (Neptune plus)**	*used for conversion*	**-0.14 ± 0.06 *4***	**0.41 ± 0.12 *5***	**-1.03 ± 0.13 *120***	**-1.00 ± 0.10 *21***	**-1.24 ± 0.13 *26***
Tacail et al., 2014[34]	MCICPMS (Neptune plus)		-0.12 ± 0.07 *11*	0.41 ± 0.06 *2*	-0.96 ± 0.14 *17*	-1.05 ± 0.07 *9*	
Colla et al., 2013[50]	MCICPMS (Neptune plus)	-0.49 ± 0.02 *2*					
Heuser and Eisenhauer 2008[48]	TIMS (TRITON)	-0.50 ± 0.15 *56*			-1.02 ± 0.12 *142*		
Heuser et al., 2011[6]	TIMS (TRITON; Mainz Lab)				-1.03 ± 0.04 *n.a.*		
Heuser et al., 2011[6]	TIMS (TRITON; Münster Lab)				-0.98 ± 0.04 *n.a.*		
Hindshaw et al., 2011[49]	TIMS (TRITON)	-0.49 ± 0.14 *46*					
Hippler et al., 2003[51]	TIMS (TRITON)			0.42 ± 0.07 *n.a.*			
Holmden et al., 2010[52]	TIMS (TRITON)			0.41 ± 0.03 *13*			
Melin et al., 2014[7]	TIMS (TRITON)			0.41 ± 0.02 *55*			
Page et al., 2008[53]	TIMS (MAT262)			0.49 ± 0.09 *15*			
Reynard et al., 2010[5]	MCICPMS (Nu plasma)	-0.57 ± 0.18 *38*		0.44 ± 0.16 *13*			
Skulan et al., 2007[54]	TIMS (VG354)			0.49 ± 0.08 *10*			
Wieser et al., 2004[37]	MCICPMS (Neptune)			0.36 ± 0.11 *54*			
Average of litterature data		**-0.52 ± 0.08** (2SD)	**-0.12 ± 0.07** (2SD)	**0.43 ± 0.08** (2SD)	**-1.00 ± 0.07** (2SD)	**-1.05 ± 0.07** (2SD)	

Table 3: **$\delta^{44/42}Ca_{ICP}$ (‰) of literature and measured SOL mode standards.** Given with 2SD and number *n* of replicates in italic (n.a.: not available). $\delta^{44/42}$Ca values are given relatively to ICP Ca Lyon Standard. Standard literature values published with respect to SRM915a were converted to SRM915b using a $\delta^{44/42}Ca_{SRM915a}$ = 0.37 ‰.[5,48-50] The - 0.14 ‰ $\delta^{44/42}Ca_{ICP}$ measured value of SRM915b was then used to convert literature values to ICP.

4.2. LA mode results

A total of 857 laser ablation analyses were carried out throughout 3 sessions, lasting 3 to 5 days each. As explained in section 3.2., the ^{87}Sr/^{86}Sr radiogenic ratio used for correction of Sr interferences was set at 0.7103. HAPp2-SPS, analysed 192 times, is the material with the highest Sr levels of the dataset ($^{87}Sr^{2+}/^{44}Ca^{+}$ of about 3.8 x 10^{-3}). Its $\delta^{44/42}Ca_{SRM}$ value was better corrected for (i.e. minimized difference between LA and SOL $\delta^{44/42}Ca_{SRM}$ values) when using a $f_{Sr^{2+}}$ mass discrimination coefficient of 1.1, which was set as the default value for the entire dataset. HAPp2-SPS displayed a $\delta^{44/42}Ca_{SRM}$ value of 1.06 ± 0.05 ‰ (2SE, n = 192) in the LA mode and yielded a value of 1.07 ± 0.01 ‰ (2SD, n = 2) in the SOL mode.

Exponential mass discrimination coefficient for corrected Ca isotope ratios in instrument (f_{Ca}) yielded an average value of 1.70 and was stable through time. Machine induced mass fractionation displayed a mean value of 4 % per amu.[38] These observations were identical to measured values in the SOL mode and indicate a similar instrumental isotopic fractionation of Ca in both modes.

		A. SOLUTION MODE								B. LA MODE							
	Sample ID	d-cusp mm	n	$\delta^{44/42}$Ca ‰ SRM	$\delta^{44/42}$Ca ‰ ICP	$\delta^{44/42}$Ca 2SD	$\delta^{43/42}$Ca ‰ SRM	$\delta^{43/42}$Ca ‰ ICP	$\delta^{43/42}$Ca 2SD	d-cusp mm	n	$\delta^{44/42}$Ca ‰ SRM	$\delta^{44/42}$Ca 2SD	$\delta^{44/42}$Ca 2SE	$\delta^{43/42}$Ca ‰ SRM	$\delta^{43/42}$Ca 2SD	$\delta^{43/42}$Ca 2SE	$^{87}Sr^{2+}/^{44}Ca^{+}$
Igneous Apatites	BRM	-	4	0.98	-0.26	± 0.07	0.50	-0.14	± 0.15		36	1.49	± 0.56	0.10	0.78	± 0.33	0.06	1.1E-03
	BRZa	-	6	1.09	-0.15	± 0.10	0.58	-0.06	± 0.06		65	1.52	± 0.88	0.11	0.85	± 0.45	0.06	9.0E-04
	DUR	-	11	0.75	-0.49	± 0.08	0.39	-0.25	± 0.07		65	1.66	± 0.69	0.09	0.99	± 0.36	0.04	1.4E-03
	MD1	-	6	1.13	-0.11	± 0.16	0.58	-0.06	± 0.10		90	1.59	± 0.66	0.07	0.84	± 0.38	0.04	1.0E-03
	MRCa	-	4	0.59	-0.65	± 0.08	0.31	-0.33	± 0.07		95	1.54	± 0.56	0.06	0.81	± 0.33	0.03	2.1E-03
Tooth Enamel	BMM3	0.60	9	-0.31	-1.55	± 0.19	-0.16	-0.80	± 0.13	0.60	27	-0.34	± 0.81	0.16	-0.06	± 0.38	0.07	5.3E-04
	HPME	-	4	-0.18	-1.42	± 0.02	-0.09	-0.72	± 0.05	-	32	-0.36	± 0.76	0.14	-0.05	± 0.43	0.08	2.9E-04
	BME1	-	3	-0.85	-2.09	± 0.07	-0.40	-1.03	± 0.08	-	16	-0.63	± 1.16	0.31	-0.23	± 0.62	0.17	2.2E-04
	BMC BMCa 5sx	1.06	4	-1.09	-2.33	± 0.13	-0.57	-1.21	± 0.09	1.20	9	-0.93	± 0.82	0.32	-0.36	± 0.57	0.22	2.3E-04
	BMCa 6sx	1.33	4	-1.15	-2.39	± 0.06	-0.59	-1.22	± 0.07									
	BMCa 7sx	2.15	2	-1.15	-2.39	± 0.07	-0.61	-1.25	± 0.06	2.31	6	-1.10	± 0.90	0.47	-0.44	± 0.66	0.34	2.6E-04
	BMCa 8sx	2.47	4	-1.11	-2.35	± 0.16	-0.55	-1.19	± 0.13									
	BMCa 9sx	3.62	4	-1.02	-2.27	± 0.15	-0.51	-1.15	± 0.11	3.62	5	-1.17	± 0.51	0.32	-0.46	± 0.31	0.19	2.7E-04
	BMC average			**-1.11**	**-2.35**	**± 0.10**	**-0.57**	**-1.20**	**± 0.08**	-	**20**	**-1.04**	**± 0.72**	**0.17**	**-0.41**	**± 0.50**	**0.12**	
	PBC PBCa 1sx	0.65	4	-0.96	-2.20	± 0.13	-0.52	-1.16	± 0.10	0.65	7	-0.98	± 0.92	0.43	-0.40	± 0.55	0.25	2.4E-04
	PBCa 3sx	1.99	3	-1.10	-2.34	± 0.01	-0.69	-1.33	± 0.10	1.99	4	-1.18	± 0.69	0.55	-0.47	± 0.37	0.30	2.4E-04
	PBCa 4sx	3.27	5	-0.96	-2.20	± 0.09	-0.49	-1.13	± 0.05	3.27	6	-0.78	± 0.79	0.41	-0.29	± 0.41	0.21	2.4E-04
	PBC average			**-1.01**	**-2.25**	**± 0.16**	**-0.57**	**-1.21**	**± 0.21**	-	**17**	**-0.96**	**± 0.84**	**0.21**	**-0.38**	**± 0.46**	**0.12**	
	VBI VBIa 10sx	2.33	2	-0.92	-2.16	± 0.04	-0.50	-1.13	± 0.29	2.33	18	-0.89	± 0.84	0.21	-0.35	± 0.43	0.11	2.9E-04
	VBIa 11sx	1.24	3	-0.73	-1.97	± 0.07	-0.36	-1.00	± 0.02	1.24	18	-0.76	± 0.84	0.21	-0.29	± 0.51	0.13	2.9E-04
	VBIa 12sx	0.25	3	-1.24	-2.48	± 0.04	-0.63	-1.27	± 0.03	0.45	18	-1.00	± 0.64	0.16	-0.40	± 0.41	0.10	2.9E-04
	VBI average			**-0.96**	**-2.20**	**± 0.52**	**-0.50**	**-1.13**	**± 0.27**	-	**56**	**-0.89**	**± 0.78**	**0.10**	**-0.35**	**± 0.44**	**0.06**	
LA Stds	SRM1400 powder		26	0*	-1.24	± 0.13	0*	-0.64	± 0.16		-	-	-	-	-	-	-	-
	SRM1400-SPS		11	0*	-1.18	± 0.16	0*	-0.57	± 0.10		-	-	-	-	-	-	-	-
	SRM1400-gold		-	0*	-	-	0*	-	-		24	0.12	± 0.68	0.14	0.15	± 0.37	0.08	8.7E-04
	HAPp1-SPS		2	1.10	-0.14	± 0.06	0.59	-0.04	± 0.00		31	1.11	± 0.77	0.14	0.73	± 0.42	0.08	2.7E-04
	HAPp2-SPS		2	1.07	-0.17	± 0.01	0.51	-0.12	± 0.08		192	1.06	± 0.64	0.05	0.58	± 0.45	0.03	3.8E-03

Table 4: **Measured $\delta^{44/42}$Ca and $\delta^{43/42}$Ca of samples and standards for SOL and LA mode analyses.** Weighted means of $\delta^{44/42}$Ca and $\delta^{43/42}$Ca are given in ‰ together with number *n* of replicates and 2SD values. SOL mode results are presented relatively to ICP Ca Lyon and to SRM1400, for which conversion was performed by using measured composition of SRM1400 ($\delta^{44/42}Ca_{ICP}$ = - 1.24 ± 0.13 ‰ and $\delta^{43/42}Ca_{ICP}$ = - 0.64 ± 0.16 ‰). LA mode results are expressed relatively to SRM1400-SPS bracketing standard and are presented with 2SE values defined as $2SE = t \times SD/\sqrt{n}$, where t is derived from the Student's t-distribution at 95 % confidence. The d-cusp column corresponds to the distance in mm to the tip of the cusp of spatially sampled teeth.

In order to verify the absence of major isobaric interference, results in the LA mode were plotted in $ln(^{43}Ca/^{42}Ca)$ *vs* $ln(^{44}Ca/^{42}Ca)$ diagrams after each sequence allowing the verification of correct mass-dependent fractionation. When summarized in a $\delta^{43/42}Ca_{SRM}$ *vs* $\delta^{44/42}Ca_{SRM}$ diagram (Fig. 1B), averaged results in the LA mode fall on a line displaying a strong correlation ($R^2 = 0.9963$) and a 0.491 ± 0.013 (2SE) slope, in good agreement with predicted slope of 0.507, according to the mass dependent fractionation exponential law. However, a 0.096 ± 0.014 (2SE) offset at origin reveals a systematic limited bias most probably due to an uncorrected isobaric interference affecting the $^{43}Ca^{+}$ beam. All analyses obtained in the LA mode are presented along with their corresponding values obtained in the SOL mode in Table 4.

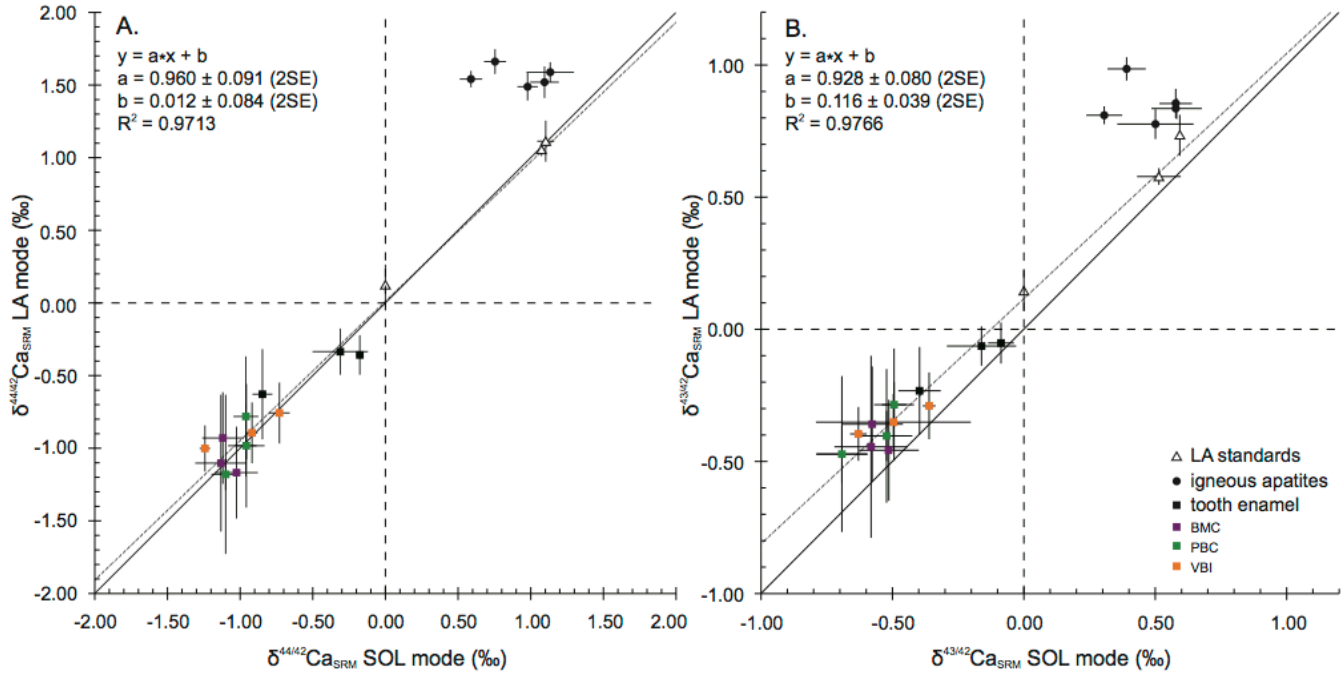

Figure 2: **LA mode *vs* SOL mode Ca isotope composition for $\delta^{44/42}Ca_{SRM}$ (A) and $\delta^{43/42}Ca_{SRM}$ (B) expressed in ‰ relatively to SRM1400.** Dashed lines correspond to regression lines, black lines correspond to 1:1 lines and error bars are 2SD in SOL mode and 2SE in LA mode. Regression calculations were performed on all samples and standards except FAP.

5. Discussion

5.1. LA-SOL modes correlations

Considering the $^{44}Ca/^{42}Ca$ ratio, the values in the LA mode for all samples except FAP compare well with those in the SOL mode (Fig. 2A), resulting in a 1:1 correlation and demonstrating a global agreement between SOL and LA mode analyses. The regression line displays a squared correlation coefficient of 0.9713, a null offset at origin (0.012 ± 0.084 ‰, 2SE) and a slope of 0.960 ± 0.091 (2SE), statistically identical to 1. Isotopic analyses in the LA mode of the sintered standards HAPp1-SPS and SRM1400-gold yield values in agreement with those in the SOL mode. The $\delta^{44/42}Ca_{SRM}$ value of HAPp1 is 1.11 ± 0.14 ‰ (2SE, n = 31) in the LA mode and 1.10 ± 0.06 ‰ (2SD, n = 2) in the SOL mode. This standard contains more than 10 times less Sr than HAPp2 ($^{87}Sr^{2+}/^{44}Ca^{+}$ ratio of 2.7×10^{-4} and 3.8×10^{-3} for HAPp1 and HAPp2, respectively). The $\delta^{44/42}Ca_{SRM}$ value of HAPp2 is 1.07 ± 0.01 ‰ (2SD, n = 2) in the SOL mode and 1.06 ± 0.05 (2SE, n = 192) in the LA mode. The fact that HAPp1 and HAPp2 display the same Ca isotopic ratio in both the SOL and LA modes suggests that the doubly charged Sr interference correction is efficient in this range of Sr levels. The belt sintered SRM1400-gold secondary standard, which must have the same Ca isotopic composition as SRM1400-SPS, displayed expected null $\delta^{44/42}Ca_{SRM}$ composition when measured in the LA mode (0.12 ± 0.14 ‰, 2SE, n = 24).

Igneous fluorapatites are tightly clustered and shifted from the 1:1 line, both for $^{44}Ca/^{42}Ca$ and $^{43}Ca/^{42}Ca$ ratios (Fig. 2). This reveals a difference of behaviour between igneous apatites in the one hand and enamel and sintered apatites in the other hand. Igneous apatites, which have false $\delta^{44/42}Ca_{SRM}$ values by about 0.40 to 1.00 ‰, do not display any correlation when plotted in the LA-SOL diagrams (Fig. 2A and 2B). This group is entirely composed of igneous centimetric monocrystalline FAP, all of which are richer in Sr than the rest of the dataset, with the exception of HAPp2. An inadequacy in the calculation of the Sr correction

could be at the source of the discrepancies between the results obtained in the SOL and the LA modes.

Considering now the $^{43}Ca/^{42}Ca$ ratio, the values in the LA mode of all samples except FAP compare well with those in the SOL mode but are systematically offset by about + 0.1 ‰ (Fig. 2B). Precisely, the regression line displays a squared correlation coefficient of 0.9766, an offset at origin of 0.116 ± 0.039 ‰ (2SE) and a slope of 0.928 ± 0.080 (2SE). The systematic offset between the SOL and the LA modes suggests that an uncorrected interference, probably linked to Sr double charge, permanently affects the $^{43}Ca/^{42}Ca$ ratio in the LA mode.

5.2. Doubly charged Sr interferences corrections

Mass fractionation is the process by which isotopes are transmitted in the mass spectrometer according to their mass, given the exponential law relationship:

$$f = \ln (r/R) / \ln (M_1/M_2) \qquad \text{Eq. [3]}$$

where f is the fractionation factor, M_1 and M_2 being the mass of two isotopes, r their measured ratio and R their true ratio.[38] Equation [2] implies that the value of f_{Sr}^{2+} is needed for the calculation of the Ca isotope intensities corrected for doubly charged Sr interferences. As already mentioned, the value of f_{Sr}^{2+} was evaluated by minimizing the corrected $^{44}Ca/^{42}Ca$ value of the HAPp2-SPS sample to its true value (*i.e.* measured without sizeable Sr thanks to the wet chemistry of the SOL mode). This value, calculated to be 1.1, was further applied to whole set of analysis. However, this value is different from that measured for f_{Ca}^{+}, which is equal to 1.7. Behaviours of doubly charged elements are not described for instrumental mass-fractionation in the literature. The significant difference found here between f_{Sr}^{2+} and f_{Ca}^{+} suggests that instrumental fractionation laws are different for single charged and doubly

charged elements. In addition, the $^{87}Sr/^{86}Sr$ ratio, being measured (r) or true (R), may vary from a sample to another depending on the inheritance of radiogenic ^{87}Sr issued from radioactive disintegration of ^{87}Rb. Taken together, approximations in the values of the $^{87}Sr/^{86}Sr$ and f_{Sr}^{2+} parameters can lead to mis-corrected $\delta^{44/42}Ca$ and $\delta^{43/42}Ca$ values. To evaluate the extent of such possible mis-corrections, we performed calculations of the error made on the $\delta^{44/42}Ca$ and $\delta^{43/42}Ca$ values given varying Sr interference intensities ($^{87}Sr^{2+}/^{44}Ca^{+}$) and varying correcting parameters, namely radiogenic Sr ratio ($^{87}Sr/^{86}Sr$) and Sr mass fractionation factor (f_{Sr}^{2+}). The results are shown in Supplementary Figure S2A to S2H. In general, the error made on the $\delta^{44/42}Ca$ value does not reach 0.05 ‰ (per amu) until the value of $^{87}Sr^{2+}/^{44}Ca^{+}$ reaches 10^{-3}, whatever the values of f_{Sr}^{2+} (Fig. S2A) and $^{87}Sr/^{86}Sr$ (Fig. S2C). However, in the same $^{87}Sr^{2+}/^{44}Ca^{+}$ range of values, the error on the $\delta^{43/42}Ca$ value is 3 to 4 times higher (Fig. S2B and S2D) than calculated for $\delta^{44/42}Ca$. Indeed, the $^{42}Ca/^{84}Sr$ and $^{43}Ca/^{86}Sr$ isotopes abundances ratios are about 1.2 and 0.01, respectively, demonstrating that the $^{43}Ca^{+}$ beam is at least 100 times more interfered than the $^{42}Ca^{+}$ beam. Variations of the f_{Sr}^{2+} and $^{87}Sr/^{86}Sr$ values do not have influence on the slope of $\delta^{43/42}Ca$ *vs* $\delta^{44/42}Ca$ mass fractionation line, until $^{87}Sr^{2+}/^{44}Ca^{+}$ reaches 0.05, which is a very high ratio (Fig. S2E and S2G). Therefore, deviation of the slope of the regression line from theoretical value is not a relevant means to assess whether doubly charged Sr interferences have been corrected accurately. Conversely, variations of the f_{Sr}^{2+} and $^{87}Sr/^{86}Sr$ values strongly influence the offset at origin of the $\delta^{43/42}Ca$ *vs* $\delta^{44/42}Ca$ mass fractionation line, even for $^{87}Sr^{2+}/^{44}Ca^{+}$ below 5×10^{-4} (Fig. S2F and S2H). A deviation of ± 0.4 unit in the f_{Sr}^{2+} correcting value modulates the offset at origin by about 0.1 ‰ (per amu) with a $^{87}Sr^{2+}/^{44}Ca^{+}$ ratio of 10^{-3}. Our observed offset at origin of ~ 0.1 ‰ (Fig. 2B) with typical $^{87}Sr^{2+}/^{44}Ca^{+}$ ratios of 2×10^{-4} - 10^{-3} corresponds to an error on the value of f_{Sr}^{2+} of about 0.2 unit, which is compatible with the suspected variability of mass fractionation factor f .[e.g 25] An inadequate value set for the $^{87}Sr/^{86}Sr$ ratio

also influences the offset at origin of the $\delta^{43/42}Ca$ *vs* $\delta^{44/42}Ca$ mass fractionation line: a deviation of ± 0.002 unit in the $^{87}Sr/^{86}Sr$ value modulates the offset at origin by about 0.05 ‰ (per amu) with a $^{87}Sr^{2+}/^{44}Ca^{+}$ of 10^{-3}. Heterogeneities of the $^{87}Sr/^{86}Sr$ ratio in the suite of FAP due to varying Sr radiogenic components could thus explain the scattering observed in the $\delta^{43/42}Ca$ *vs* $\delta^{44/42}Ca$ diagram using the LA mode (Fig. 2A and 2B). However, when the dataset is corrected using more or less radiogenic $^{87}Sr/^{86}Sr$ ratios, this does not ameliorate the accuracy of the FAP $\delta^{44/42}Ca$ values (Fig. 3). For instance, the Durango apatite remains inaccurate by + 0.45 ‰ (per amu), when varying its correcting $^{87}Sr/^{86}Sr$ ratio from 0.7103 default value to 0.7050, which is slightly less radiogenic than its true $^{87}Sr/^{86}Sr$ ratio of 0.7063.[41] Furthermore, theoretical calculations presented in Fig. S2A and S2B show that inaccurate f_{Sr}^{2+} values induce opposite errors in $\delta^{44/42}Ca$ and $\delta^{43/42}Ca$, resulting in distinct distributions for the two ratios in the δCa_{SOL}-δCa_{LA} diagram. Thus, an erroneous estimation of f_{Sr}^{2+}can not account for the observed systematic discrepancies for igneous apatites. Finally, matrix effects possibly affect the analysis of Ca isotopes in igneous apatites in the LA mode. Igneous apatites are fluorapatites containing up to 4 % of fluorine.[45] This high concentration is in contrast with that of SRM1400 bone ash standard, which is ~ 1250 $mg.g^{-1}$, and with that of the in house precipitated apatites (HAPp1 and HAPp2), which are hydroxylapatites completely free of fluorine. The difference of texture between the monocrystalline igneous apatites and the sub-micrometric crystallized enamel and sintered standards can also be of importance regarding Ca isotopic fractionation during laser ablation, transport and plasma ionisation.

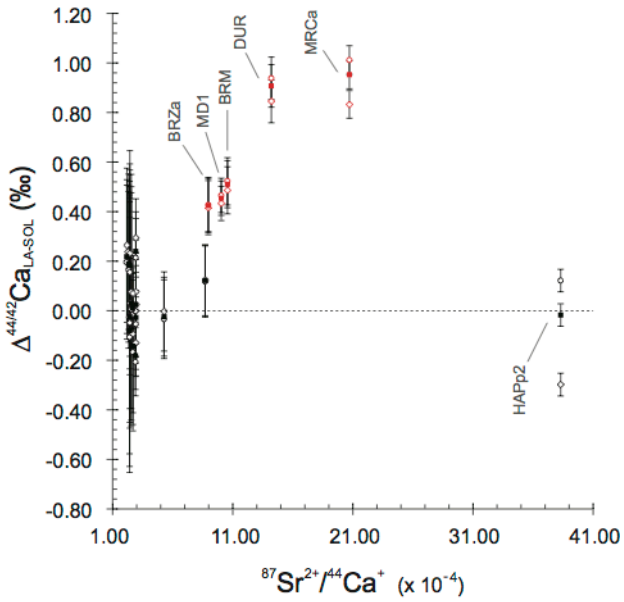

Figure 3: **$\Delta^{44/42}Ca_{LA\text{-}SOL}$ as a function of $^{87}Sr^{2+}/^{44}Ca^{+}$ signal ratios.** Distance to SOL mode value $\Delta^{44/42}Ca_{LA\text{-}SOL}$ is defined as $\delta^{44/42}Ca_{SRM\text{-}LA} - \delta^{44/42}Ca_{SRM\text{-}SOL}$ (in ‰). For each sample and standard, the $\Delta^{44/42}Ca_{LA\text{-}SOL}$ has been calculated with LA mode $\delta^{44/42}Ca_{SRM}$ values obtained using three different $^{87}Sr/^{86}Sr$ correcting ratios, namely 0.7050, 0.7103 and 0.7130. Red points correspond to FAP. Error bars are 2SE.

5.3. Variations of Ca isotopic compositions in enamel

The wisdom and deciduous teeth analysed for Ca isotope compositions exhibit significantly different bulk $\delta^{44/42}Ca$ values in the SOL mode. Deciduous teeth are depleted in Ca heavy isotopes, with an average $\delta^{44/42}Ca_{SRM}$ of – 0.98 ± 0.21 ‰ (2SD, 4 teeth). These are significantly different from the two wisdom teeth (- 0.24 ± 0.19 ‰, 2SD), corresponding to a shift of about + 0.74 ± 0.29 ‰ from deciduous to wisdom teeth. The LA mode also accounts for an average shift of + 0.53 ± 0.36 ‰ between deciduous and wisdom teeth, respectively being, – 0.88 ± 0.36 ‰ (2SD, 4 teeth) and - 0.35 ± 0.03 ‰ (2SD, 2 teeth). The significantly ^{44}Ca-depleted compositions of deciduous teeth are likely to be the result of the influence of milk in the early life diet because the Ca isotope composition of human milk has a particularly ^{44}Ca-depleted composition, with $\delta^{44/42}Ca_{ICP}$ values around - 1.68 ± 0.43 ‰ (2SD, n = 4)[8] while European diet is thought to lie around - 1.08 ‰ in average.[46] The observed shift

between the $\delta^{44/42}$Ca values of deciduous and wisdom teeth is thus likely to be induced by a transition from a milk based diet to a plant and meat based diet.

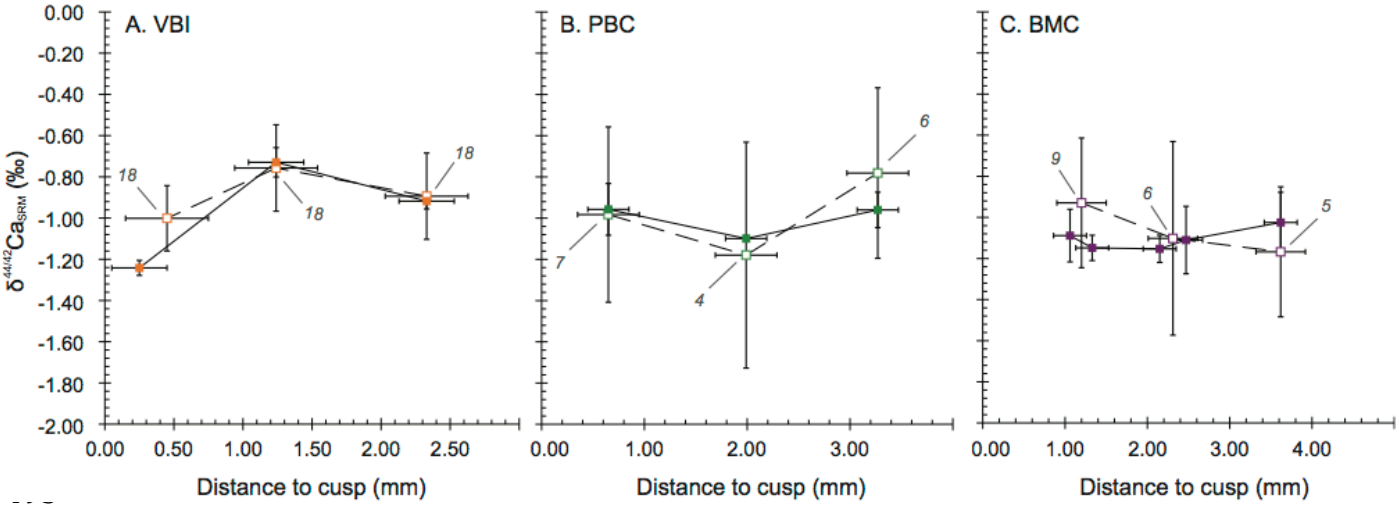

Figure 4: **VBI (A), PMC (B) and BMC (C) deciduous tooth cusp to cervix profiles: $\delta^{44/42}Ca_{SRM}$ as a function of distance to top cusp for both SOL and LA modes.** Empty squares are LA mode analyses and full squares correspond to SOL mode analyses with MicroMill sampling. The number of LA mode analyses is given next to each LA mode $\delta^{44/42}Ca_{SRM}$**.** Vertical error bars are 2SE for LA mode and 2SD for SOL mode. Horizontal error bars correspond to approximate width of sampling area.

The results of micro-sampled deciduous tooth enamel are presented in Fig. 4, where the $\delta^{44/42}Ca_{SRM}$ values acquired in the SOL and LA modes are plotted with respect to the distance to the tip of the tooth cusp. The results obtained in the SOL mode reveal no distinguishable variation within tooth enamel for the PBC and BMC canines (Fig. 4B and 4C), while VBI incisor displays a strong variation in $\delta^{44/42}Ca_{SRM}$ values, with a shift from - 1.24 ± 0.04 ‰ to - 0.73 ± 0.07 ‰ from 0.25 to 1.24 mm distance to cusp (Fig. 4A). The $\delta^{44/42}Ca_{SRM}$ results in the LA mode are consistent with those in the SOL mode, although the reduced number of analyses per point (4 to 9) is responsible for some apparent discrepancies between the two modes for the PBC and BMC canines. For all tooth samples, discrepancy of the results between the SOL and LA modes can also be explained by local variations, because all laser rasters could not be processed exactly where the associated micro-samplings have been. The $\delta^{44/42}Ca_{SRM}$ variations in VBI along enamel growth axis is most probably linked to dietary or

physiological transitions during the formation of deciduous incisors. The mineralisation of human deciduous incisors is achieved at least 6 months before the complete formation of canine crowns, after birth.[47] This early formation of incisors could explain the recording of early transitions in Ca sources.

Conclusion

We demonstrate in the article that the laser ablation technique can be used to measure Ca isotope compositions in biological, but not igneous, apatites. However, only the $\delta^{44/42}$Ca ratio yields accurate values, the $\delta^{43/42}$Ca ratio being systematically offset by about 0.1 ‰. We stress that appropriate correction of Sr double charge interferences and use of matrix-matched standards are of crucial importance to obtain accurate $\delta^{44/42}$Ca values. We also show using calculations that the offset at origin of the $\delta^{43/42}$Ca *vs* $\delta^{44/42}$Ca regression line is the most sensible outcome when optimizing the correction of Sr double charge interferences. Despite the use of an extensive correction of the interferences due to Sr double charges, which considers the fractionation factor of Sr^{2+} and the value of the $^{87}Sr/^{86}Sr$ as variables, we were not able to find accurate $\delta^{44/42}$Ca values for the igneous apatites. We hypothesize that the mismatch is probably due to different matrix texture and composition between the sintered microcrystalline fluorine-free standards and the macrocrystalline fluorine-rich samples.

The present study opens up perspectives for the measurements of Ca isotopes in fossil vertebrates with a minimum of sample preparation and destruction. However, providing adapted matrix-matched strategy, the technique can also be applied to carbonate Ca calcified tissues, such as shells, tests and otoliths.

Acknowledgements

The Laser Ablation device was funded by the Fonds Recherche of the Ecole Normale Supérieure de Lyon and this study was supported by the Bullukian and the Mérieux foundations. The authors are grateful to B. Reynard and G. Bonnefont for SPS sintering experiments. F. Albarède and E. Albalat are thanked for their help and advice on MC-ICPMS theory.

Bibliography

1 J. Skulan, D. J. DePaolo and T. L. Owens, *Geochim. Cosmochim. Acta*, 1997, **61**, 2505–2510.

2 J. Skulan and D. DePaolo, *Proc. Natl. Acad. Sci. U. S. A.*, 1999, **96**, 13709–13713.

3 M. T. Clementz, P. Holden and P. L. Koch, *Int. J. Osteoarchaeol.*, 2003, **13**, 29–36.

4 D. DePaolo, *Rev. Mineral. Geochemistry*, 2004, **55**, 255–288.

5 L. M. Reynard, G. M. Henderson and R. E. M. Hedges, *Geochim. Cosmochim. Acta*, 2010, **74**, 3735–3750.

6 A. Heuser, T. Tütken, N. Gussone and S. J. G. Galer, *Geochim. Cosmochim. Acta*, 2011, **75**, 3419–3433.

7 A. D. Melin, B. E. Crowley, S. T. Brown, P. V Wheatley, G. L. Moritz, F. T. Yit Yu, H. Bernard, D. J. DePaolo, A. D. Jacobson and N. J. Dominy, *Am. J. Phys. Anthropol.*, 2014, **154**, 633–43.

8 N.-C. Chu, G. M. Henderson, N. S. Belshaw and R. E. M. Hedges, *Appl. Geochemistry*, 2006, **21**, 1656–1667.

9 S. Graham, N. Pearson, S. Jackson, W. Griffin and S. Y. O'Reilly, *Chem. Geol.*, 2004, **207**, 147–169.

10 I. Horn, R. Schoenberg and F. von Blanckenburg, *J. Anal. At. Spectrom.*, 2006, **21**, 211.

11 J. Košler, R. Pedersen, C. Kruber and P. Sylvester, *J. Anal. At. Spectrom.*, 2006, **21**, 214.

12 I. Horn, F. von Blanckenburg, R. Schoenberg, G. Steinhoefel and G. Markl, *Geochim. Cosmochim. Acta*, 2006, **70**, 3677–3688.

13 I. Horn and F. von Blanckenburg, *Spectrochim. Acta Part B At. Spectrosc.*, 2007, **62**, 410–422.

14 F.-X. D'Abzac, A.-M. Seydoux-Guillaume, J. Chmeleff, L. Datas and F. Poitrasson, *J. Anal. At. Spectrom.*, 2012, **27**, 108.

15 C. K. I. Sio, N. Dauphas, F.-Z. Teng, M. Chaussidon, R. T. Helz and M. Roskosz, *Geochim. Cosmochim. Acta*, 2013, **123**, 302–321.

16 W. Dziony, I. Horn, D. Lattard, J. Koepke, G. Steinhoefel, J. a. Schuessler and F. Holtz, *Chem. Geol.*, 2014, **363**, 101–113.

17 F.-X. d'Abzac, A. D. Czaja, B. L. Beard, J. J. Schauer and C. M. Johnson, *Geostand. Geoanalytical Res.*, 2014, **38**, 293-309.

18 M. Oeser, S. Weyer, I. Horn and S. Schuth, *Geostand. Geoanalytical Res.*, 2014, **38**, 311–328.

19 E. D. Young, R. D. Ash, A. Galy and N. S. Belshaw, *Geochim. Cosmochim. Acta*, 2002, **66**, 683–698.

20 P. E. Janney, F. M. Richter, R. A. Mendybaev, M. Wadhwa, R. B. Georg, E. B. Watson and R. R. Hines, *Chem. Geol.*, 2011, **281**, 26–40.

21 J. A. Schuessler and F. Von Blanckenburg, *Spectrochim. Acta - Part B At. Spectrosc.*, 2014, **98**, 1–18.

22 S. E. Jackson and D. Günther, *J. Anal. At. Spectrom.*, 2003, **18**, 205–212.

23 P. R. Craddock, O. J. Rouxel, L. A. Ball and W. Bach, *Chem. Geol.*, 2008, **253**, 102–113.

24 J. Míková, J. Košler and M. Wiedenbeck, *J. Anal. At. Spectrom.*, 2014, **29**, 903.

25 M. D. Norman, M. T. McCulloch, H. S. C. O'Neill and G. M. Yaxley, *J. Anal. At. Spectrom.*, 2006, **21**, 50.

26 T. Hinners, R. Hughes, P. Outridge, W. J. Davis, K. Simon and D. R. Woolard, *J. Anal. At. Spectrom.*, 1998, **13**, 963–970.

27 M. M. Schweissing and G. Grupe, *J. Archaeol. Sci.*, 2003, **30**, 1373–1383.

28 A. Ugarte, N. Unceta, C. Pécheyran, M. A. Goicolea and R. J. Barrio, *J. Anal. At. Spectrom.*, 2011, **26**, 1421.

29 V. Balter and C. Lécuyer, *Geochim. Cosmochim. Acta*, 2004, **68**, 423–432.

30 E. Champion, *Acta Biomater.*, 2013, **9**, 5855–75.

31 V. Balter, P. Telouk, B. Reynard, J. Braga, F. Thackeray and F. Albarède, *Geochim. Cosmochim. Acta*, 2008, **72**, 3980–3990.

32 V. Balter and B. Reynard, *Bone*, 2008, **42**, 229–34.

33 V. Balter, J. Braga, P. Télouk and J. F. Thackeray, *Nature*, 2012, 10–12.

34 T. Tacail, E. Albalat, P. Télouk and V. Balter, *J. Anal. At. Spectrom.*, 2014, **29**, 529.

35 M. Schiller, C. Paton and M. Bizzarro, *J. Anal. At. Spectrom.*, 2012, **27**, 38.

36 J.-I. Kimura, T. Takahashi and Q. Chang, *J. Anal. At. Spectrom.*, 2013, **28**, 945–957.

37 M. E. Wieser, D. Buhl, C. Bouman and J. Schwieters, *J. Anal. At. Spectrom.*, 2004, **19**, 844.

38 C. Maréchal, P. Télouk and F. Albarède, *Chem. Geol.*, 1999.

39 F. Albarède, P. Telouk, J. Blichert-Toft, M. Boyet, A. Agranier and B. Nelson, *Geochim. Cosmochim. Acta*, 2004, **68**, 2725–2744.

40 Y. Asahara, T. Tanaka and H. Kamioka, *Earth Planet. Sci. Lett.*, 1995, **133**, 105–116.

41 M. S. A. Horstwood, J. A. Evans and J. Montgomery, *Geochim. Cosmochim. Acta*, 2008, **72**, 5659–5674.

42 P. Stille, A. D. Schmitt, F. Labolle, M. C. Pierret, S. Gangloff, F. Cobert, E. Lucot, F. Guéguen, L. Brioschi, M. Steinmann and F. Chabaux, *Comptes Rendus - Geosci.*, 2012, **344**, 297–311.

43 R. S. Hindshaw, B. Bourdon, P. A. E. Pogge von Strandmann, N. Vigier and K. W. Burton, *Earth Planet. Sci. Lett.*, 2013, **374**, 173–184.

44 M. S. Fantle, *Geochim. Cosmochim. Acta*, 2015, **148**, 378–401.

45 P. L. Roeder, D. Macarthur, X. D. Ma, G. R. Palmer and a. N. Mariano, *Am. Mineral.*, 1987, **72**, 801–811.

46 A. Heuser and A. Eisenhauer, *Bone*, 2010, **46**, 889–96.

47 S. Hillson, Dental Anthropology, Cambridge University Press, Cambridge, 1996

48 A. Heuser and A. Eisenhauer, in *Geostandards and Geoanalytical Research*, 2008, vol. 32, pp. 311–315.

49 R. S. Hindshaw, B. C. Reynolds, J. G. Wiederhold, R. Kretzschmar and B. Bourdon, *Geochim. Cosmochim. Acta*, 2011, **75**, 106–118.

50 C. A. Colla, J. Wimpenny, Q.-Z. Yin, J. R. Rustad and W. H. Casey, *Geochim. Cosmochim. Acta*, 2013, **121**, 363–373.

51 D. Hippler, A.-D. Schmitt, N. Gussone, A. Heuser, P. Stille, A. Eisenhauer and T. F. Nägler, *Geostand. Geoanalytical Res.*, 2003, **27**, 13–19.

52 C. Holmden and N. Bélanger, *Geochim. Cosmochim. Acta*, 2010, **74**, 995–1015.

53 B. Page, T. Bullen and M. Mitchell, *Biogeochemistry*, 2008, **88**, 1–13.

54 J. L. Skulan, T. D. Bullen, A. D. Anbar, J. E. Puzas, L. C. Shackelford, A. LeBlanc and S. M. Smith, *Clin. Chem.*, 2007, **53**, 1153–5.